Available online at www.sciencedirect.com
ScienceDirect
Journal of the European Ceramic Society 31 (2011) 1015–1025
www.elsevier.com/locate/jeurceramsoc

Original Article

Thermal stability in air of surface nitrided 3Y-TZP

J. Valle *, A. Mestra, M. Anglada

Departament de Ciència del Materials i Enginyeria Metallúrgica, Universitat Politècnica de Catalunya, Av. Diagonal 647, 08028 Barcelona, Spain

Received 9 April 2010; received in revised form 12 November 2010; accepted 27 November 2010
Available online 12 January 2011

Abstract

Surface nitriding can be optimised to protect 3Y-TZP against hydrothermal degradation and at the same time to keep the mechanical properties of the surface and the bulk unchanged. However, thermal stability is a concern that can limit its use above room temperature. In this work, surface nitrided 3Y-TZP was heat treated in air at 200, 400, 600 and 800 °C for 8 h. Treatments up to 600 °C did not change microstructure and Vickers hardness, but heating at 800 °C produced surface defects, inner cracks and grain decohesion, conducing to a dramatic decrease in mechanical strength. Heat treatments above 400 °C led to an increase of indentation fracture toughness and to a complete loss of the hydrothermal degradation resistance achieved by nitriding.

Keywords: Zirconia; ZrO_2; Surfaces; Thermal properties; Mechanical properties

1. Introduction

Ceramics of zirconia doped with yttria are used in many applications, ranging from gas sensors to biomedical implants, because they have a good combination of mechanical and functional properties. The main feature of zirconia doped with 3% molar yttria (3Y-TZP) is transformation toughening due to stress assisted tetragonal–monoclinic (t–m) transformation.[1] However, this transformation can be also triggered by reaction with water from the environment, causing degradation of the surfaces in contact with water after exposure for relatively short times, and a severe drop in strength after long times. This phenomenon, which is referred as low temperature degradation (LTD), causes a dramatic drop of mechanical properties of 3Y-TZP, being an important drawback for its application in biomedical implants[2] and in restorative dentistry.[3]

Since its knowledge, many attempts have been carried out to avoid LTD: reduction of grain size, increase of stabiliser content and coatings, among many others.[4] All these methods imply changes in surface or bulk properties, bringing the need to make additional considerations. A promising method that could protect the material without significantly affecting the mechanical properties is surface modification. In the past, this has been carried out by post-sintering heating in a stabiliser powder bed in order to incorporate stabilising cations into the surface.[5] Another method is to incorporate nitrogen anions by nitriding.[6] By doping the surface either with stabilising cations or with nitrogen, in general, the effect is to generate oxygen vacancies, which stabilise the surface region and increase the resistance to degradation. Nitriding has been successfully tried before, but a layer of cubic or t′ phase with equiaxial and columnar morphologies is formed at the surface, which has lower fracture toughness than tetragonal 3Y-TZP.[7,8] The layer is very brittle, with hardness similar to cubic zirconia, and its fracture toughness can be hardly measured by indentation due to chipping.

As N^{3-} has a relative large mobility at high temperature, it becomes an important concern to determine the effect of temperature on the stability of nitrogen doped zirconia in air. In this sense, there are two works that have dealt with this aspect. Chung et al.[6] annealed surface nitrided 2Y-TZP at 200 °C for 400 h, without observing any change in mechanical strength compared to as sintered material. Feder et al.[8] performed nitriding of 2.5Y-TZP at temperatures of 1650 °C for 1 and 2 h, and after cooling they observed a surface t′ layer and underneath a tetragonal zone with a large grain size which decreases in the depth direction. After heat treatments in air at temperatures from 400 °C to 800 °C, a large fraction of this zone underwent phase transformation accompanied by microcracking.

* Corresponding author. Tel.: +34 934054454; fax: +34 934016706.
E-mail address: Jorge.antonio.valle@upc.edu (J. Valle).

0955-2219/$ – see front matter © 2010 Elsevier Ltd. All rights reserved.
doi:10.1016/j.jeurceramsoc.2010.11.029

In this study, the variables of nitriding process (temperature and dwell time) were selected to reduce the nitrogen doping of the surface to the extent that there is no generation of other phases at the surface but still increasing the resistance of 3Y-TZP to LTD. Therefore, the aim of this study is to investigate the stability in air of surface nitrided 3Y-TZP when nitriding does not produce the aforementioned fragile layer, but the tetragonal microstructure with small grain size is retained.

2. Experimental procedure

The starting material was 3Y-TZP powder (Tosoh Co., Japan). The powder was isostatically pressed in a cylindrical polymeric mould at 200 MPa. The green rods were then sintered at 1450 °C for 2 h, with a rate of heating and cooling of 3 °C/min. The cylinders were cut into discs 2 mm thick, and polished to have a mirror-like surface.

The preparation of samples for nitriding was performed by coating the whole surface of the discs (named AS for "as sintered") with 0.70 g of ZrN powder, and compacting in a uniaxial metallic mould to ensure consistence (using a load of 10 kN). The ensembles were heat treated in a tubular furnace at 1400 °C for 1 h, with 100% nitrogen flux of 1 l/min.

Although for biomedical applications the resistance to LTD of 3Y-TZP is focused to human body temperature (37 °C) in body fluids, the evaluation of the resistance to LTD was carried out under more severe conditions by performing accelerated hydrothermal degradation tests (autoclave, 131 °C, steam atmosphere, 30 h.). On the other hand, the heat treatments for stability analysis of nitrogen doped 3Y-TZP were done in air at 200 °C, 400 °C, 600 °C and 800 °C for 8 h. To verify the combined effect of temperature and time on morphology changes, further treatments were performed at 800 °C for 30 min and at 600 °C for 24 h.

The microstructural changes were analyzed on the surface by X-ray diffraction (Bruker AXS D8 Advance), with CuKα radiation, in a range of $2\theta = 24–78°$, in $\theta–2\theta$ and 1° grazing angle mode. Also the surface and cross section were studied locally by micro-Raman spectroscopy (Jovin Ivon T64000), using a 532 nm argon laser with a power of 800 mW, and taking spectra from 100 to 700 cm^{-1}. Morphological features were observed first by optical microscopy (Olympus Lext), with a polarized light filter to highlight the surface relieves. Details of the generated cracks and fracture surfaces were observed by SEM (Jeol JT-5600). Atomic Force Microscopy imaging (Digital Instruments AFM Dimension 3100), in tapping mode, was performed on the surface in order to determine the shape and dimensions of the appearing uplifts. Polished cross sections were observed by SEM and Laser Scanning Confocal Microscopy (LSCM, Olympus Lext).

Hardness was measured by Vickers indentation with a load of 9.8 N (1 kg). Moreover, 294 N (30 kg) imprints were made to measure indentation fracture toughness by the method of Niihara et al.[9] Nano Berkovich indentations (MTS Nanoindenter XP) of 150 nm depth were performed along the cross section to evaluate possible changes in hardness after the heat treatments. Young modulus by means of nanoindentation was calculated by the Oliver and Pharr method[10] in continuous stiffness measurement. Biaxial bending strength was evaluated by the ball on three ball method.[11]

3. Results

3.1. Nitrided material

The starting material for nitriding was prepared according to ASTM standard F-1873, which accounts for 3Y-TZP requisites for biomedical applications. The sintering process produced a 99% dense material with an average grain size of 0.3 μm, and open porosity less than 0.1%. After nitriding for 1 h at 1400 °C the phase remained tetragonal, with a moderate increase in grain size, as shown in Fig. 1.

3.2. Damage characteristics

The most noticeable feature of nitrided zirconia after heat-treatments in air was the change of the morphology of the surface. As sintered zirconia in air had a white colour, that turned grey after nitriding. By contrast, the samples air heat-treated at 400 and 600 °C did not show any difference at the surface with respect to the nitrided material. However, the surface of the samples heat-treated at 800 °C had a significant change: the colour of the surface turned to be whiter and there was the appearance of round shaped surface uplifts, many of them accompanied by arched cracks with an average length of 30 μm (see Figs. 2 and 3).

Samples heat treated at 600 °C only showed blistering at the borders of the discs, and for 400 °C there was no change observable. In Fig. 2b it can be appreciated that the blistering at the border of the sample is finer and more abundant that in the centre. The formed cracks during heat-treatment in air at 800 °C were readily observable by optical microscopy; however, a polarized light filter was needed to reveal the shape of the uplifts. Concerning the additional heat treatments mentioned above, the sample subjected at 800 °C for 30 min showed a similar amount and distribution of defects like the treatment at 800 °C for 8 h. In one treated at 600 °C for 24 h there was also generation of defects of the same shape that those found at 800 °C, but in minor amount.

From the optical examinations of samples heat treated at 800 °C (Fig. 2), there seems to be a relation between the concentration of nitrogen and the amount and size of the defects. During nitriding, the flux of nitrogen is higher at the border of the discs; in this zone it was generated a transformed layer with bigger grain size, similar to that observed by Feder et al.[8] in cylindrical specimens. In this outer annular surface of about 300 μm in width, the defects are finer and numerous (Fig. 2b); but their number decreases in the centre of the disc (Fig. 2a), and their diameter length, as observed in the surface, is commonly higher than 20 μm.

To analyze the nature of the uplifts, they were observed by SEM. In Fig. 3a it can be appreciated that the uplifts are originated by an emerging crack, whose faces are displaced in the direction perpendicular to the surface. The sample has been tilted

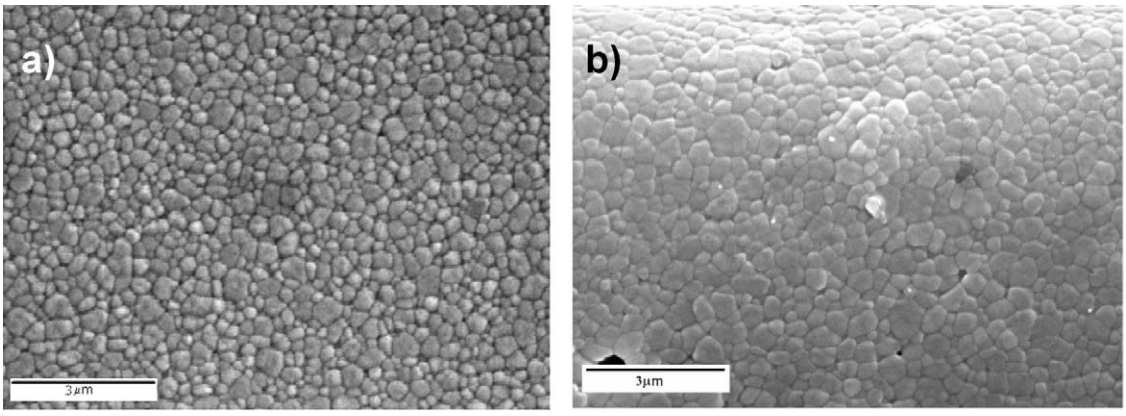

Fig. 1. (a) Surface microstructure of as sintered 3Y-TZP and (b) cross section of nitrided material.

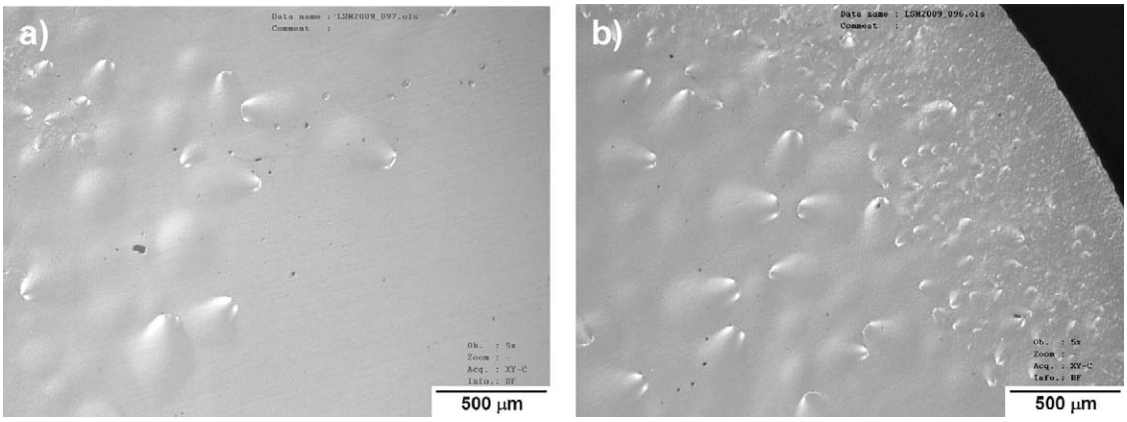

Fig. 2. Polarized light optical image of the surface of nitrided 3Y-TZP, after heat treatment in air at 800 °C for 8 h: (a) centre of the disc and (b) border.

40° to make noticeable the uplift effect, given that its height is in the order of the grain size. A detail of the crack is presented in Fig. 3b, where it can be observed clearly the contour of the grains at both sides of the crack. It is shown that the formation of the crack is via intergranular fracture.

In order to determine the dimensions of the defects, these were analyzed by AFM, as shown in Fig. 3. It can be observed in Fig. 4a that the edges of the crack have a steep difference in height (z axis) of 250 nm. Immediately after the step, the height of the uplift decreases linearly along the direction perpendicular to the crack. In the direction parallel to the crack, the shape of the defect is curve shaped, and its height decreases until it disappears.

In order to establish the extent of the crack into the bulk, a cross section of the disc, perpendicular to the crack, was ground and polished. Fig. 5a depicts schematically the orientation grinding of sectioning to reveal the features of the defect inside the bulk. Fig. 5b–d shows different details of the cross section of the

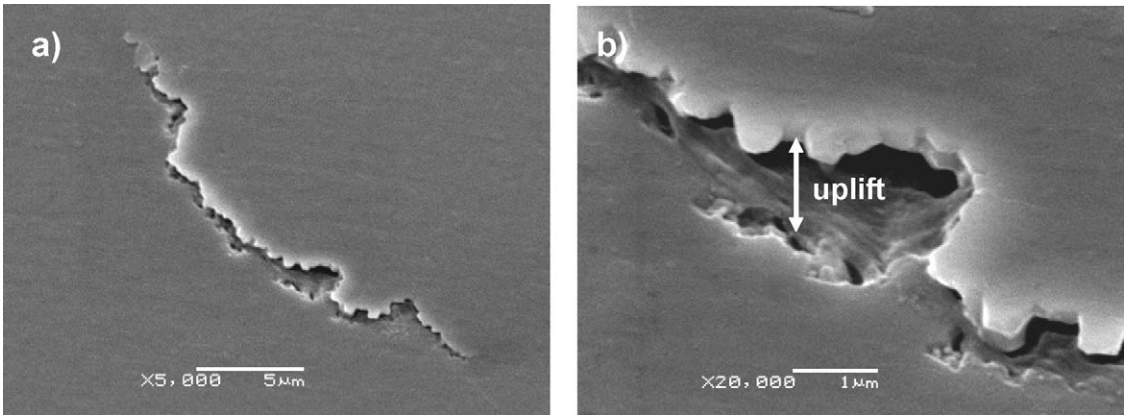

Fig. 3. SEM images of (a) crack accompanying uplift. (b) Detail of the crack showing intergranular fracture.

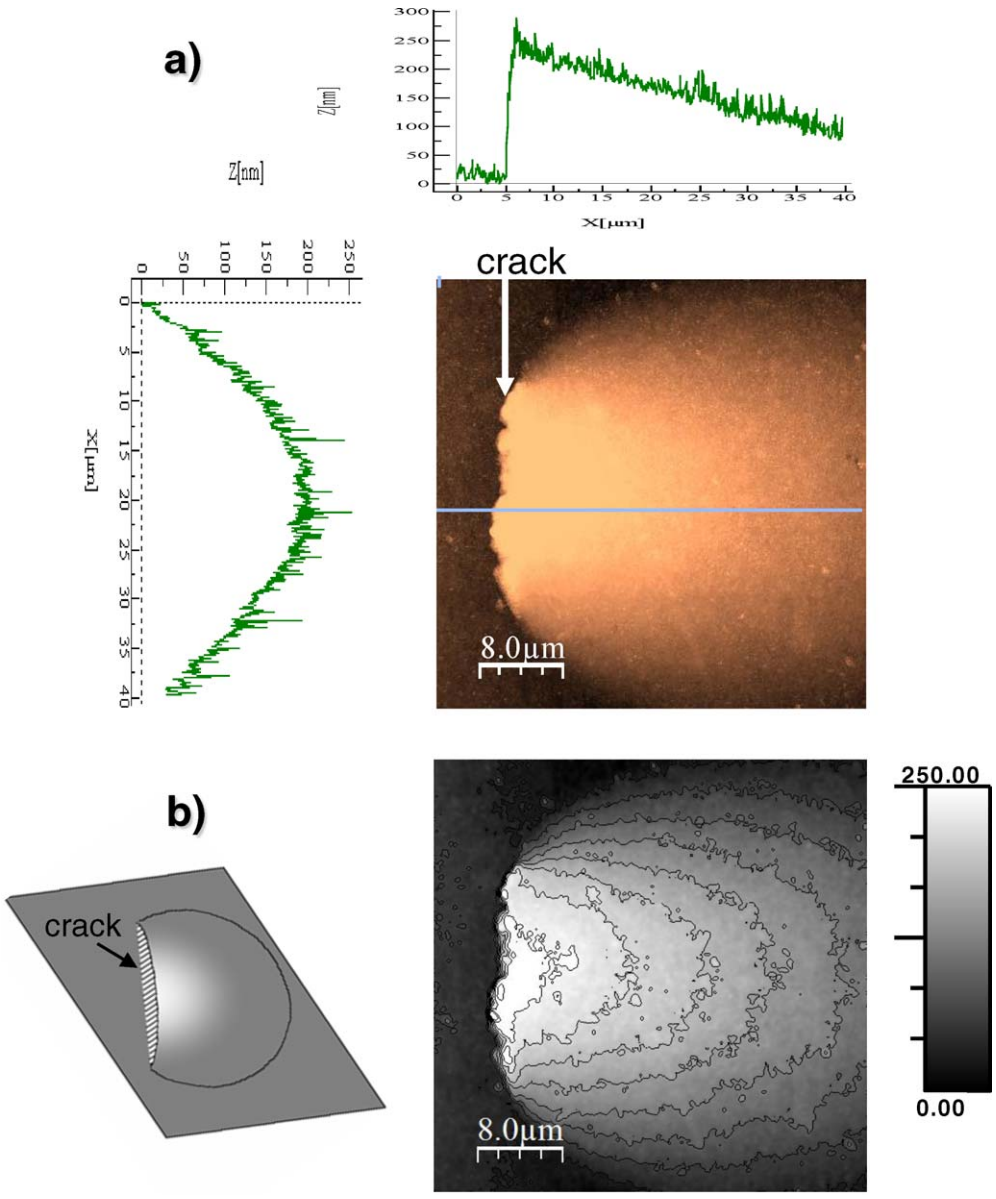

Fig. 4. AFM images of the produced defects after heat treatments at 800 °C. (a) Linear profiles perpendicular and parallel to the crack. (b) Contoured shape. The distance between contour lines corresponds to a difference in height of 30 nm.

defect. It can be appreciated (Fig. 5b) that the crack extends into the bulk up to a depth of 50 μm, forming an angle of approximately 30° with respect to the surface. The trajectory is straight until it reaches 30 μm of depth, then it turns tortuous and more parallel to the surface, until the defect disappears. Fig. 5c shows a detail of the crack closer to the upper surface, indicating that it could have a semi conical shape. The propagation of the crack to the bulk is also intergranular, as observed in Fig. 5d.

To investigate the effect of heat-treatments in air on the microstructure, beyond the formation of the previously described defects, fracture morphology was also observed by SEM in disc specimens fractured by biaxial flexion in a ball on three ball fixture. There are three zones of different appearance in the fracture surfaces shown in Fig. 6. The upper zone (Fig. 6b), closest to the surface, is characterized by a high intergranular decohesion, as the contour of the grains is clearly observed. This section is followed by an intermediate zone (Fig. 6c), where intergranular decohesion is present in a lesser degree, and the cohesion between grains seems to be stronger since transgranular brittle fracture features can be observed. Finally in the bulk (Fig. 6d) intergranular decohesion is minimal and brittle fracture is the main mechanism of failure.

3.3. Microstructure

The level of nitrogen in the surface after nitriding could not be measured by using electron microprobe analysis. Therefore it is assumed that it is below the detection limit of the equipment (about 0.8 wt% for nitrogen). XRD patterns taken both before and after nitriding did not show any measurable change in lattice parameters. To reveal subsurface features, a polished cross section of the sample heat treated at 800 °C was observed by LSCM

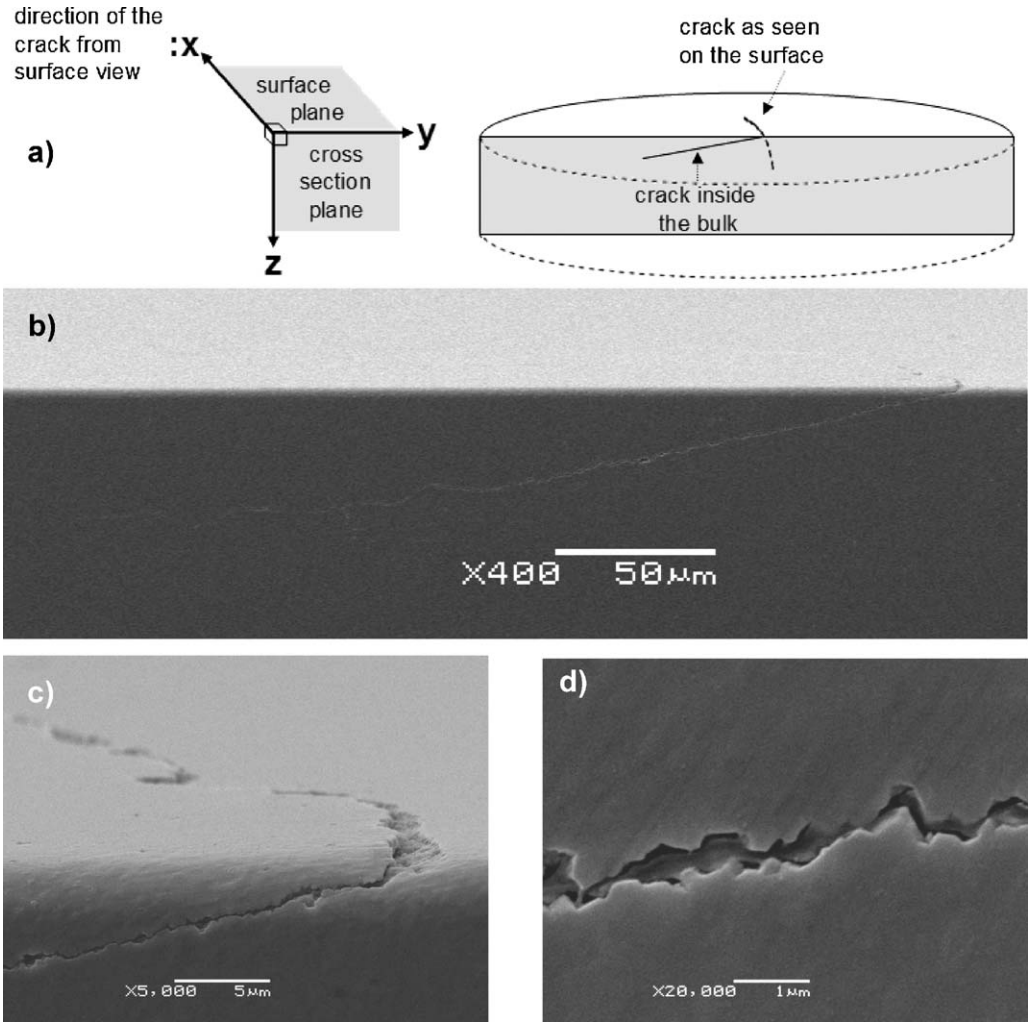

Fig. 5. Cross section of a crack formed during treatments at 800 °C. (a) Schematic view of the section. (b) Overview of the whole defect. (c) Detail of the near surface. (d) Detail of the defect showing intergranular propagation.

(Fig. 7a) and SEM (Fig. 7b). A large number of intergranular cracks are observed only near the upper surface in Fig. 7a, while Fig. 7b shows an enlarged view SEM image of one of them. Raman spectroscopy was employed in order to make a local analysis of the possible phase changes related to the generation of uplifts, specifically tetragonal to monoclinic transformation associated with microcracking. Fig. 8 shows Raman spectra collected at several places of the samples, including measurements made on the surface and in the cross section at different distances from the upper surface to the core of the disc, is it to say, different depths. Concerning the external surface, for 800 °C treatment the laser beam was focussed on the centre of the disc, right on an cracks uplift; and for the rest of the treatments measurements were taken also from the centre, but in plain zones because of the absence of uplifts. In depth, spectra for all treatments were carried out in polished cross sections of the discs, starting from the upper surface close to the centre of the disc, and along the depth direction. There was no monoclinic phase detected in uplifted, plain zones, or cross sections, in any of the heat-treated specimens.

3.4. Mechanical properties

To investigate the effect of the cracks on mechanical properties, hardness, mechanical strength and indentation fracture toughness were measured. In the case of hardness, both Berkovich nanoindentation of 1.5 μm depth and Vickers indentations of 9.8 N and 294 N were performed. Table 1 shows that values remain unaltered with respect to untreated and non nitrided zirconia, except for the specimens heat-treated at 800 °C, for which surface hardness has slight lower values. Specimens heat-treated at 800 °C fractured while being indented at 294 N, and also the strength measured in flexure by the ball on three balls test was about three times less that for the rest of tested conditions. Indentation fracture toughness for all conditions is shown in Fig. 9.

Also hardness and Young's modulus were examined at several depths in the cross section of the discs, starting from the upper surface, by means of Berkovich nanoindentations (Fig. 9). It can be seen that these parameters remained steady with the depth of analysis.

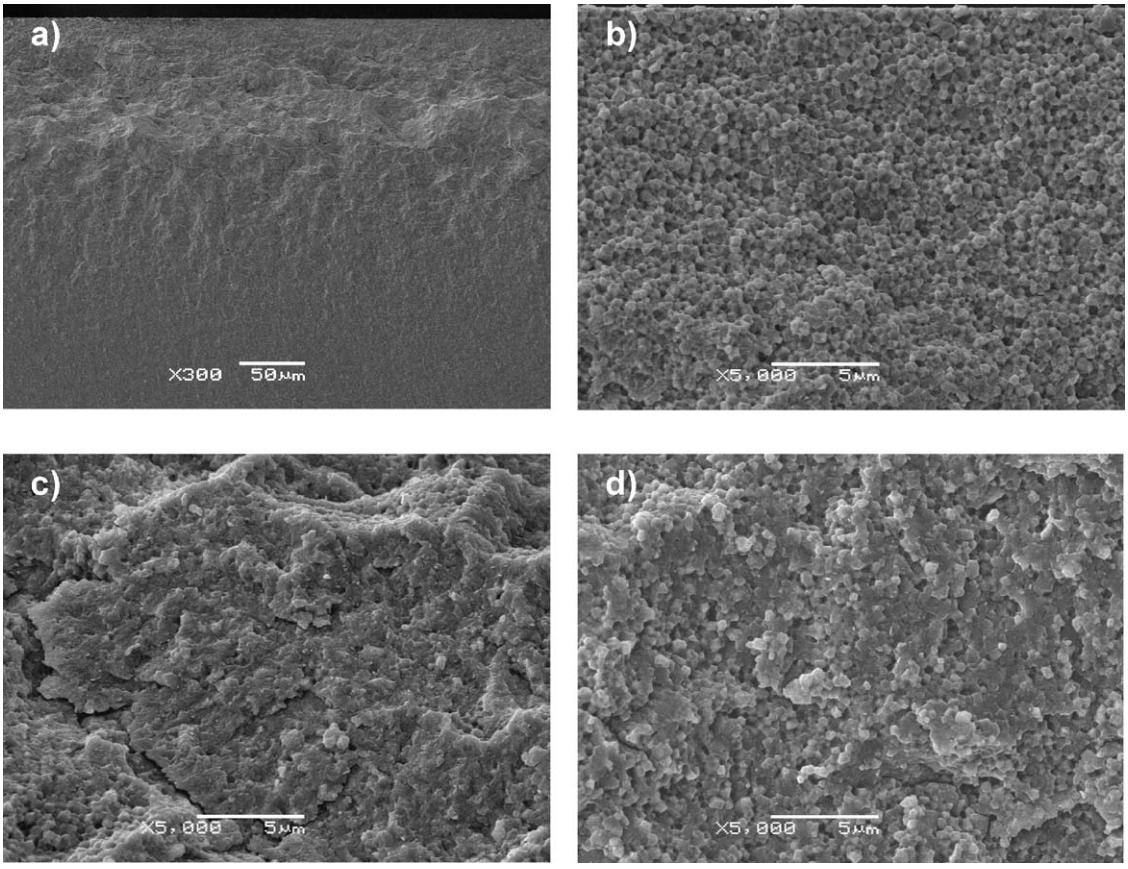

Fig. 6. Fracture surface of heat treated discs. (a) Overview of the three morphologies observed: (b) upper zone, (c) intermediate zone and (d) bulk.

Indentation fracture toughness of heat treated samples (Fig. 10) showed a slight increase as compared to AS and nitrided material. To assess possible overestimations coming from the application of the method of measurement, a range of indentation loads from 19.6 to 294 N was applied. The formula used is that of Niihara et al., since c to a ratio for all performed measurements is less than 3.5, thus indicating Palmqvist cracks[9]:

$$K_{IC} = 0.018H\sqrt{a}\left(\frac{E}{H}\right)^{0.4}\left(\frac{c}{a}-1\right)^{-0.5} \quad (1)$$

where H is the Vickers hardness, c is the length from the centre of the indentation to the crack tip, E is the Young modulus (210 GPa for 3Y-TZP), and a is the half diagonal of the imprint. This method is not valid when c/a is smaller or close to one, and is valid up to a c/a ratio of about 3.5 (transition from Palmqvist to radial crack). When c/a ratio approaches to 1, the calculated K_{IC} increases significantly, giving an overestimation. However it is clear that the value obtained calculated by Eq. (1) is always higher for heat treated nitrided samples.

To find out more about the increase of indentation fracture toughness of the surface with the temperature of heat treat-

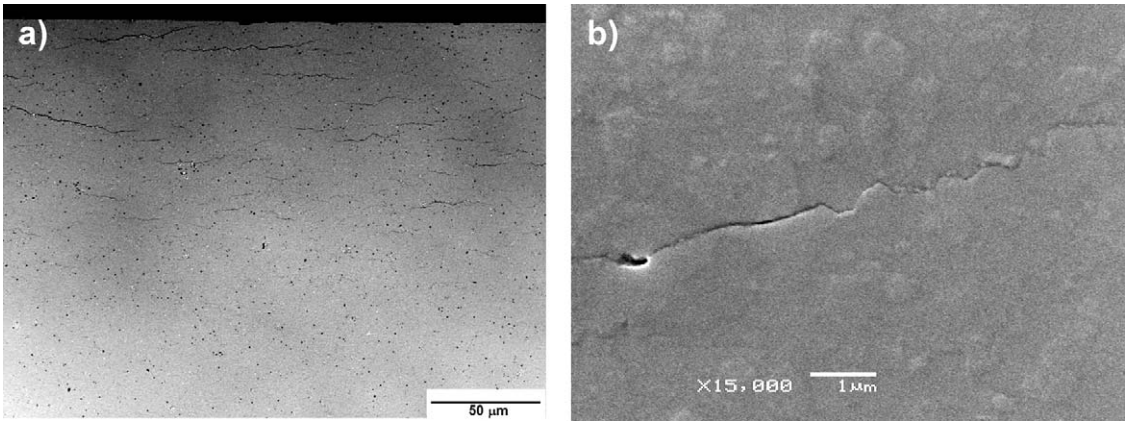

Fig. 7. Polished cross section of material heat treated at 800 °C. (a) LSCM image showing high amount of horizontal fissures and (b) SEM detail of a crack denoting inter-intragranular propagation.

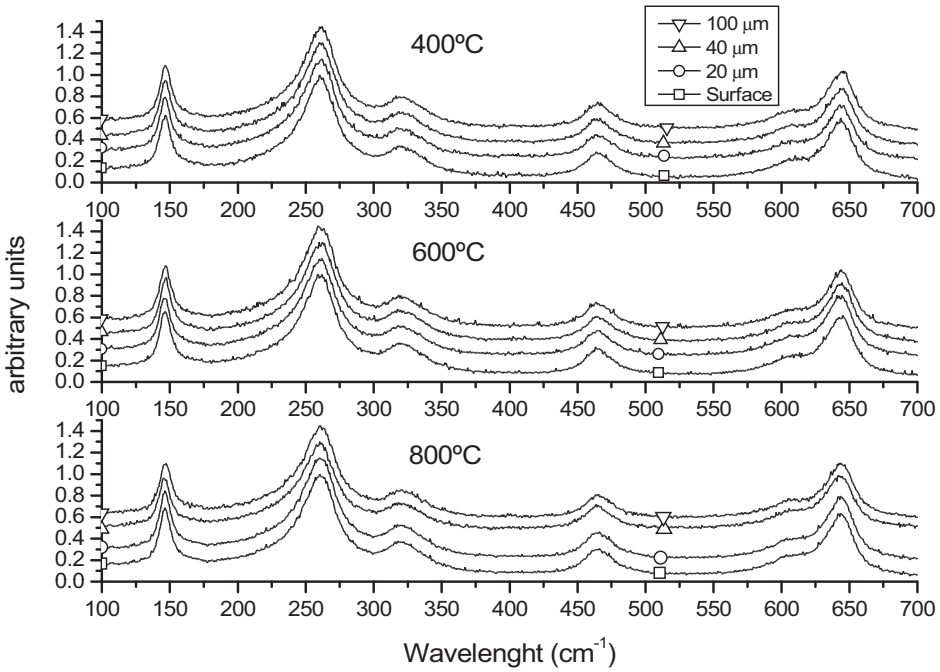

Fig. 8. Raman spectra collected at different depths in cross section of heat treated samples.

ments, SEM images of HV5 originating cracks were taken (Fig. 11). It can be seen that AS cracks propagate like inter-transgranular straight path (common for Y-TZP). On the other hand, the behaviour turns more transgranular and tortuous when the nitrided samples are heat treated in air.

The appearance of surface defects also had an important influence on the mechanical strength of heat treated samples. The mechanical strength measured from ball on three balls tests, shown in Fig. 12, indicates that samples heat treated at 400 °C and 600 °C did not undergo changes in biaxial bending strength; however, after heat treatment at 800 °C in air (where the surface cracks appear) the strength is about one third with respect to the untreated 3Y-TZP. Due the small number of tested samples, it was not possible to establish any clear change of strength with the other heat treatments. However, measurements of the 800 °C-treated specimen were repeated several times to confirm that there is a significant decrease of strength for this specific treatment.

3.5. Resistance to hydrothermal degradation

Finally, it was obtained from autoclave ageing tests that the resistance to LTD is completely lost in air heat treated nitrided samples. XRD results shown in Fig. 13 indicate that, before air

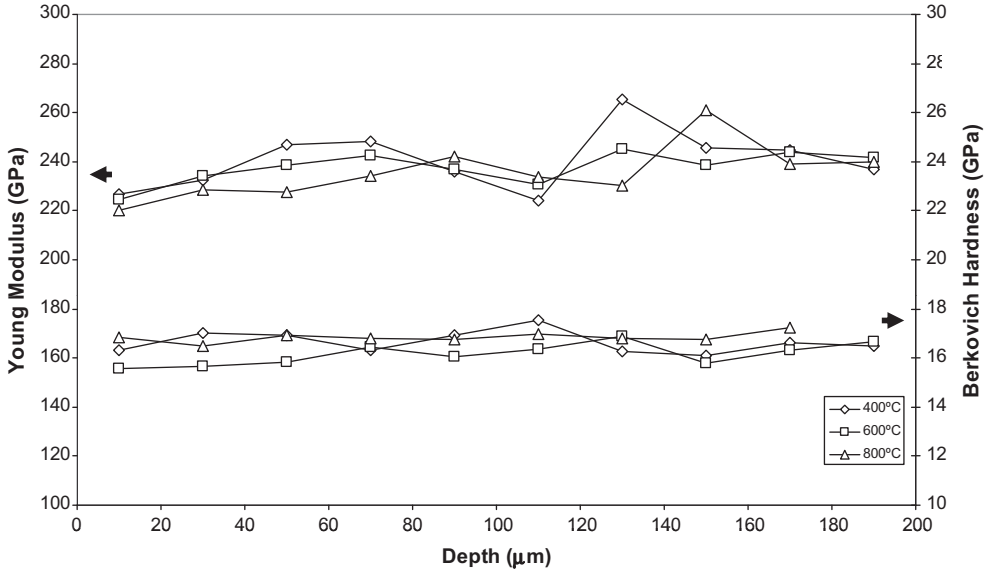

Fig. 9. Mechanical properties measured at cross section of heat treated samples.

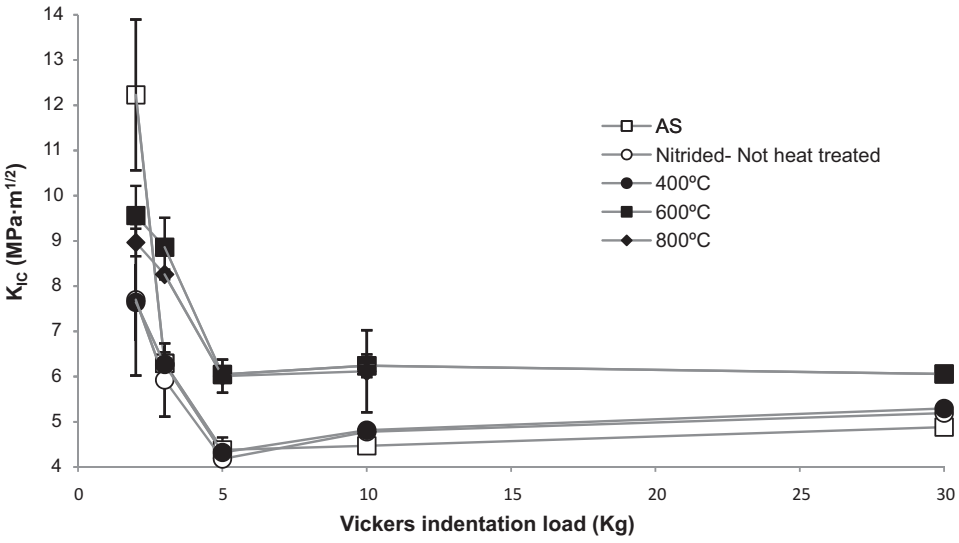

Fig. 10. Indentation fracture toughness for all conditions at different Vickers loads. Value for 800 °C at 30 kg is not shown because the sample broke during indentation.

heat treatment, the nitrided material was much more resistant to LTD compared to as-sintered samples, as expected. However, after air heat treatments over 400 °C, both nitrided and non-nitrided samples underwent similar amount of t–m transformation at the surface. Also, the material that showed surface defects disintegrated after autoclave degradation.

4. Discussion

During nitriding of zirconia, doping is assumed to occur by the reaction show by Eq. (2), written using Kroger–Vink notation[12]

$$3O_O^x + N_2 \rightarrow 2N_O' + V_O^{oo} + 1.5O_2 \quad (2)$$

The uptake of nitrogen can come from the atmosphere (must be 100% N_2 to prevent oxidation) or from nitrogen containing compounds. Darkening of zirconia is frequently related to deviation from stoichiometry due to oxygen vacancies.[13,14]

The incorporation of nitrogen during surface modification was too low to induce measurable changes of lattice parameters by XRD. According to Cheng and Thompson[15] and given that the crystalline structure did not change, the nitrogen content at the surface should be less than 0.1 wt%, in order to have a stable tetragonal structure. Deghenghi et al.[16] calculated a diffusion coefficient of 2×10^{-8} cm^2/s for nitrogen in 2Y-TZP at 1400 °C. Given the similarities of chemical composition and microstruc-

Table 1
Surface hardness measured by Berkovich nanoindentation and Vickers indentation. HV1 and HV30 correspond to indentation loads of 9.8 and 294 N, respectively.

Specification	Heat treatment (°C)	Surface hardness (GPa)
Vickers HV1	As sintered	11.7 ± 0.1
	Nitrided	13.1 ± 0.1
	400	12.8 ± 0.1
	600	12.5 ± 0.1
	800	12.4 ± 0.1
Vickers HV30	As sintered	12.8 ± 0.2
	Nitrided	13.1 ± 0.1
	400	12.7 ± 0.5
	600	12.7 ± 0.1
	800	Broke
Berkovich 1500 nm depth	As sintered	17.5 ± 0.2
	Nitrided	18.0 ± 0.1
	400	17.2 ± 0.3
	600	16.8 ± 0.2
	800	15.9 ± 0.2

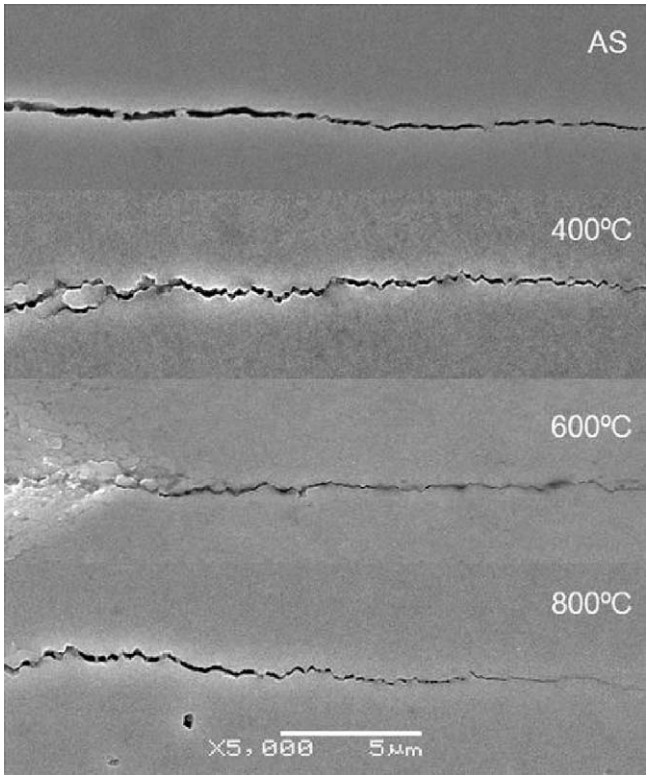

Fig. 11. Cracks originated by HV5 indentations.

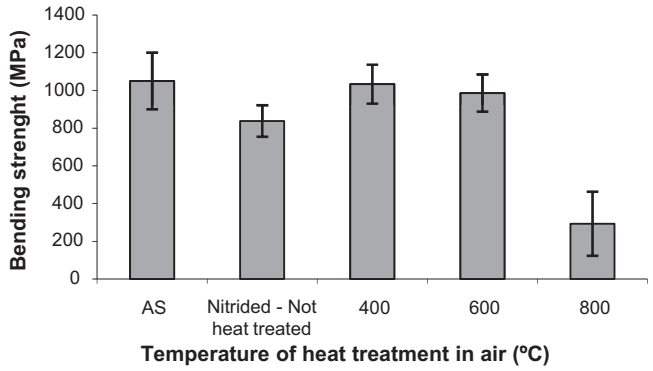

Fig. 12. Biaxial bending strength of heat treated samples.

ture before nitriding, it could be used to infer the nitrogen profile after doping in the current work. If the problem is considered as diffusion in one dimension (perpendicular to the surface) a solution of the second law of Fick can be employed (Eq. (3)):

$$\frac{C(x,t)}{C_i} = \mathrm{erfc}\left(\frac{x}{2\sqrt{Dt}}\right) \quad (3)$$

where $C(x,t)$ and C_i are, respectively, the nitrogen concentration at a given depth and at the interphase (where %N is maximum), x is the depth, D is the diffusion coefficient and t is the time of nitriding. For the nitriding process applied (1400 °C for 1 h), from the change in lattice parameter of the tetragonal phase it can be estimated that the content at the surface is less than 0.1 wt% of nitrogen, if the amount of nitrogen coming from ZrN is considered in excess and steady. In the range where the argument of the complementary error function varies between 0 and 0.5, the derivative of the function can be considered constant, and this implies that there is a linear decreasing gradient from the surface (where the %N is maximum) up to a depth of 80 μm where half of doping with respect to the surface is reached (less than 0.05 wt%).

Once nitrided, if zirconia is heated in an oxidizing atmosphere, the reaction mentioned before is reverted, and oxygen may diffuse to the interior to fill oxygen vacancies created during nitriding. In order to maintain the charge neutrality, nitrogen gas is released. This is supported by the fact that the coefficient of diffusion of N in Y-TZP[6,12] is three order of magnitude higher than for Y and Zr.[17] In addition, although nitrogen self-diffusion has almost twice the activation enthalpy of oxygen self-diffusion (about 2 and 1 eV, respectively), at temperatures close to 1000 K, nitrogen and oxygen diffusion coefficients are roughly identical.[18]

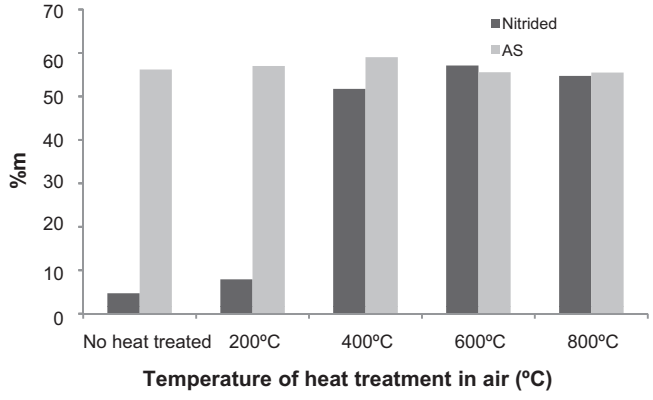

Fig. 13. Percentage of monoclinic phase detected by XRD on heat treated samples after hydrothermal ageing tests.

The fact that there was generation of uplifts in the whole surface also at 600 °C after 24 h shows that the phenomenon involved is also present at this temperature, but it is less kinetically favourable that at 800 °C.

SEM details of the generated cracks (Fig. 3) reveal an intergranular fracture. This path could be explained either by some intrinsic weakening of grain boundaries due to the presence of nitrogen, or because of the build up of pressure due to formation of nitrogen gas at these internal surfaces. Propagation of cracks in non-nitrided Y-TZP presents a mixture of intergranular and transgranular modes at low temperatures[19]; but for the heat treated material it tends to be mainly intergranular close to the surface. This is also confirmed by cross section examinations (Fig. 5), where the path of the crack follows a straight line bordering the grains only up to depths of about 30 μm, that is, the depth mainly affected by nitrogen during nitriding. Then the crack path turns more irregular in deeper regions, indicating that the grain junctions resulted less affected. This makes more difficult the propagation of the crack towards the interior of the specimen.

The generation of uplifts, whose height was measured by AFM to be around 250 nm (Fig. 4), is the evidence of a subsurface process. Grain boundary decohesion can be clearly observed in fracture surfaces (Fig. 6). It can be noticed that the change of morphology is directly related to the assumed nitrogen concentration profile induced by surface modification. During heat treatment in air, nitrogen ions could have diffused and combined at the external surface and at grain boundaries to produce molecular nitrogen. These gas molecules accumulate at grain boundaries, pores and triple points and might generate enough pressure to induce grain decohesion and to produce the previously described defects in the upper zone (Fig. 5a). As the nitrogen content decreases with depth, there is less release of nitrogen in the deeper regions affected by nitriding and the fracture appearance is less intergranular. Below 150 μm depth the nitrogen effect on the microstructure is negligible.

The interior cracks observed in LSCM and SEM images of polished cross sections (Fig. 7) were helpful to determine the integrity of the material after nitrogen release at 800 °C. These cracks also appear in the zone where the nitrogen content was high before heat treatments. The distribution and orientation of the inner cracks indicate that the surface defects could have been originated beneath the surface. Those cracks observed in Fig. 7a, originated by pressure generation, that reach the surface (the upper edge in cross section), might have propagated easier towards the surface due to the increasing grain junction weakening.

The fact that after treatment in air at the different temperatures t–m phase transformation was not detected by micro-Raman spectroscopy could be explained by the low grain size. In the

original Y-TZP t–m transformation is already much reduced to a very thin layer on the crack surfaces because of the difficulty to trigger t–m transformation when the grain size is very small. In addition, the total number of oxygen vacancies after nitriding should be larger than the original number in 3Y-TZP, if oxygen ions are replaced by nitrogen ions during nitriding. During heat treatment in air, their number should decrease but should be at least as high in the original 3Y-TZP. Therefore, there is no reason to destabilise the tetragonal structure neither from the point of view of the number of vacancies nor from an increase in grain size. As nitrogen is released when the nitrided material is heated in air, the stress to induce t–m transformation inside the grains should not increase since the amount of oxygen vacancies will be restored because of the high mobility of oxygen at 800 °C.

One possible cause of the increase of the indentation fracture toughness with the temperature of heat treatment (Fig. 10) can be inferred from Fig. 11, which shows the trajectory of indentation cracks for different test conditions. Cracks in AS specimens show a straight inter-transgranular path, typical of 3Y-TZP. However, heat treated samples show a more intergranular and tortuous pathway, which increases K_{IC}.

Properties related to the bulk behaviour such as macrohardness (Table 1) did not change with the heat treatment in air because these tests describe the average behaviour of the material in a surface zone that is much deeper than the surface layer affected by the heat-treatment. Berkovich nanoindentation shows that surface hardness increases after nitriding (as shown in Table 1), and it decreases during heat treatment. This slight decrease could be related to the presence of microcracks in the near surface. The steadiness of the nanohardness profile in cross section for 400 °C and 600 °C (Fig. 11), evidences that microstructure was not affect significantly. For 800 °C it can be explained by the small size of nanoindentations which measure only regions of healthy material.

The cause of the decrease in strength (Fig. 12) after heat-treatment in air at 800 °C is obviously the appearance of the inner and surface cracks described above. The large amount of inner fissures interacts among themselves under the applied stresses, causing the failure by a combination of at least two modes of fracture. On the contrary, for the material heat treated at lower temperatures, the strength is similar to the untreated zirconia; that is, the strength is maintained if no surface defects are created during air heat treatment.

The loss of LTD protection (shown in Fig. 13) after heat treatment in air can be explained by the reduction of the amount of vacancies in the surface. As stated before, the reversion of the nitriding reaction includes the reincorporation of oxygen in the lattice and the disappearing of anion vacancies to preserve the electrical balance. The lower the amount of vacancies, the lower the stability of tetragonal phase.[20] Presence of vacancies is determinant for hydrothermal degradation occurrence[21]; this is even more important at the surface, where the phenomenon starts. Therefore, if surface vacancies of nitrided material are reduced, it will tend to degrade like non nitrided 3Y-TZP. In addition the surface defects of the material heat treated at 800 °C meant an easier pathway for water penetration. All effects described above do not occur in nitride samples heat treated in air at 200 °C (see Fig. 13). Therefore the increase of temperature favours kinetically and thermodynamically the ionic exchange of nitrogen and oxygen at the surface of nitrided zirconia, this being detrimental to LTD resistance.

5. Conclusions

Although nitriding of 3Y-TZP at 1400 °C makes the material resistant to LTD without changing the grain size and the excellent mechanical properties of the starting material, it is concluded that:

(a) Heat-treating in air of surface nitrided 3Y-TZP at 800 °C for 8 h produces grain decohesion and surface uplifts with associated cracks. Although there is no phase or microstructural change, there is an important decrease in mechanical strength.
(b) Heat-treating at 400 °C and 600 °C for the same period of time does not affect the microstructure and Vickers hardness. There is a slight increase of indentation fracture toughness for all heat treatments, possibly related to crack deflection toughening.
(c) Defects created by exposure to air at 800 °C and change in mechanical properties are explained in terms of the substitution of nitrogen by oxygen and the production of gas nitrogen at internal surfaces.
(d) Heat treatments over 400 °C produce the loss of protection against LTD of nitrided material, which is caused by the reincorporation of oxygen and the reduction of surface anion vacancies.

Acknowledgements

The authors are grateful to E. Jimenez-Pique for helping in the nanoindentation tests, to the Spanish Ministerio de Ciencia e Innovación for financial support under the project MAT2008-03398, and J. Valle is also grateful to the Ministerio de Educación de España for receiving a FPU scholarship.

References

1. Hannink RHJ, Kelly PM, Muddle BC. Transformation toughening in zirconia-containing ceramics. *J Am Ceram Soc* 2000;**83**(3):461–87.
2. Chevalier J, Gremillard L, Deville S. Low-temperature degradation of zirconia and implications for biomedical implants. *Ann Rev Mater Res* 2000;**37**:1–32.
3. Lughi V, Sergo V. Low temperature degradation – aging – of zirconia: a critical review of the relevant aspects in dentistry. *Dent Mater* 2010;**26**:807–20.
4. Lawson S. Environmental degradation of zirconia ceramics. *J Eur Ceram Soc* 2000;**15**(6):485–502.
5. Sato T, Ohtaki S, Endo T. Improvement of thermal-stability of yttria-doped tetragonal zirconia polycrystals by doping CeO_2 on the surface. *J Mater Sci Lett* 1986;**5**(11):1140–2.
6. Chung T, Song H, Kim G. Microstructure and phase stability of yttria-doped tetragonal zirconia polycrystals heat treated in nitrogen atmosphere. *J Am Ceram Soc* 1997;**80**(10):2607–12.
7. Chung T, Lee J, Kim D. Surface nitriding of yttria-doped tetragonal zirconia polycrystals (Y-TZP): microstructural evolution and kinetics. *J Am Ceram Soc* 1999;**82**(11):3193–9.

8. Feder A, Alcalá J, Llanes L. Microstructure, mechanical properties and stability of nitrided Y-TZP. *J Eur Ceram Soc* 2003;**23**(15):2955–62.
9. Niihara K, Morena R, Hasselman DPH. Evaluation of K_{IC} of brittle solids by the indentation method with low crack-to-indent ratios. *J Mater Sci Lett* 1982;**1**(1):13–6.
10. Oliver WC, Pharr GM. An improved technique for determining hardness and elastic-modulus using load and displacement sensing indentation experiments. *J Mater Res* 1992;**7**(6):1564–83.
11. Danzer R, Harrer W, Supancic P. The ball on three balls test-strength and failure analysis of different materials. *J Eur Ceram Soc* 2007;**27**(2–3):1481–5.
12. Kroger FA, Vink HJ. Relations between the concentrations of imperfections in crystalline solids. *Solid State Phys* 1956;**3**:307–435.
13. Guo X, Sun YQ, Cui K. Darkening of zirconia: a problem arising from oxygen sensors in practice. *Sens Actuators B: Chem* 1996;**31**(3):139–45.
14. Sergo V, Schmid C, Meriani S, Evans AG. Mechanically induced zone darkening of alumina/ceria-stabilized zirconia composites. *J Am Ceram Soc* 1994;**77**(11):2971–6.
15. Cheng Y, Thompson DP. Nitrogen-containing tetragonal zirconia. *J Am Ceram Soc* 1991;**74**(5):1135–8.
16. Deghenghi G, Chung T, Sergo V. Raman investigation of the nitriding of yttria-stabilized tetragonal zirconia. *J Am Ceram Soc* 2003;**86**(1):169–73.
17. Swaroop S, Kilo M, Argirusis C, Lattice. Grain boundary diffusion of cations in 3YTZ analyzed using SIMS. *Acta Mater* 2005;**53**(19):4975–85.
18. Kilo M, Taylor MA, Borchardt G. Fast anion-conduction in oxynitrides: oxygen and nitrogen transport in (Y, Zr)–(O, N). *Diffusion Fundamentals* 2008;**8**:8.1–7.
19. Alcala J, Anglada M. Fatigue and static crack propagation in yttria-stabilized tetragonal zirconia polycrystals: crack growth micromechanisms and precracking effects. *J Am Ceram Soc* 1997;**80**(11):2759–72.
20. Kontouros P, Petzow G. Defect chemistry, phase stability and properties of zirconia polycrystals. In: Badwal SPS, Bannister MJ, Hannink RHJ, editors. *Science and technology of zirconia V*. Lancaster, Basel: Technomic; 1993. p. 30–48.
21. Guo X. Hydrothermal degradation mechanism of tetragonal zirconia. *J Mater Sci* 2001;**36**:3737–44.